Three-dimensional two-component velocity measurement of the flow field induced by the *Vorticella picta* microorganism using a confocal microparticle image velocimetry technique

Moeto Nagai,[1] Masamichi Oishi,[1] Marie Oshima,[2] Hiroshi Asai,[3] and Hiroyuki Fujita[1]
[1]*Institute of Industrial Science, The University of Tokyo, 4-6-1 Komaba, Meguro-ku, Tokyo 153-8505 Japan*
[2]*Interfaculty Initiative in Information Studies, The University of Tokyo, 4-6-1, Komaba, Meguro-ku, Tokyo 153-8505, Japan*
[3]*Advanced Research Institute for Science and Engineering, Waseda University, 3-4-1 Okubo, Shinjuku-ku, Tokyo 169-8555, Japan*

(Received 11 January 2009; accepted 27 February 2009; published online 26 March 2009)

Understanding the biological feeding strategy and characteristics of a microorganism as an actuator requires the detailed and quantitative measurement of flow velocity and flow rate induced by the microorganism. Although some velocimetry methods have been applied to examine the flow, the measured dimensions were limited to at most two-dimensional two-component measurements. Here we have developed a method to measure three-dimensional two-component flow velocity fields generated by the microorganism *Vorticella picta* using a piezoscanner and a confocal microscope. We obtained the two-component velocities of the flow field in a two-dimensional plane denoted as the *XY* plane, with an observation area of 455×341 μm^2 and the resolution of 9.09 μm per each velocity vector by a confocal microparticle image velocimetry technique. The measurement of the flow field at each height took 37.5 ms, and it was repeated in 16 planes with a 2.50 μm separation in the *Z* direction. We reconstructed the three-dimensional two-component flow velocity field. From the reconstructed data, the flow velocity field $[u_{(x,y,z)}, v_{(x,y,z)}]$ in an arbitrary plane can be visualized. The flow rates through *YZ* and *ZX* planes were also calculated. During feeding, we examined a suction flow to the mouth of the *Vorticella picta* and measured it to be to 300 pl/s. © *2009 American Institute of Physics.* [DOI: 10.1063/1.3105106]

I. INTRODUCTION

Vorticella is a microorganism categorized as a stalked ciliate protozoan. *Vorticella* has a stalk anchored onto a substrate and an array of cilia distributed around its oral region for feeding.[1] When feeding, these cilia move constantly, creating a powerful vortical flow. Suspended particles in the vicinity are sucked into this vortex and into the oral opening. It is important to examine the flow generated by a microorganism for scientific and engineering interests. From a scientific point of view, it is of great interest to study the flow generated by a microorganism in order to understand a specific biological feeding strategy. The feeding mechanism of stalked ciliates is used to collect food from the surrounding water while the cell is attached to a substrate.[2] In contrast, most macroscopic animals travel to capture food. It is not well understood why stalked ciliates produce vortexlike flows and circulate the flow for repeated uptake of bacteria, as well as the size and shape of the flow and the magnitude and composition of the inflow of suction. From an engineering viewpoint, it is necessary to characterize the flow created by a microorganism for the potential utilization of this microorganism as a microfluidic device inside microelectromechanical systems. Such devices have been successfully developed; Kim and Breuer[3,4] presented two types of active

biobased devices for micrototal analysis systems. They reported that the movement of the flagella of microorganisms enhanced mixing in a microchannel at low Reynolds numbers and could be employed as micromixers in microchannels.[3] They also demonstrated that fluid could be pumped through microchannels at speeds of as high as 25 μm/s.[4] This flow was induced by the collective motion of thousands of the self-organized flagella. The characterization of microorganismic-induced flows is indispensable for the design and application of devices based on microorganisms.

Several velocimetry methods have been applied to investigate fluid flow dynamics induced by microorganisms.[5–12] However, to our knowledge, a three-dimensional (3D) velocimetry method to measure the flows generated by microorganisms has not yet been reported. The dimensions of the measurements have been limited to two-dimensional (2D) two components. Only a few studies of flow rates around the microorganism were carried out. Vopel *et al.*[5] conducted measurements of one-dimensional one-component flows induced by ciliates with a flow microsensor. They scanned the sensor around the vicinity of a *Vorticella* and a *Zoothamnium* and obtained the linear velocity profiles of the flow. They were able to measure quantitative flow speeds with this method; however, it is inappropriate for measuring the 3D flow field while a *Vorticella* is stationary because they recorded 1000 data points at 50 Hz and averaged them, and the acquisition of the flow velocity at each point takes 20 s. Furthermore, they could not measure the water velocity at a distance smaller than 50 μm from the cell body of the *Vorticella* because the deformation of the flow field caused by the presence of the sensor tip changed the positions of the ciliates.

2D two-component measurements were conducted with two different velocimetric methods.[6–12] The first method is particle tracking velocimetry (PTV), a technique to measure the velocity of a flow-driven particle. Sleigh and Aiello applied PTV to microorganisms and followed the movement of water around the cilia of *Vorticella*[6] and *Stentor*[7] by tracing the motion of latex particles with a frame-by-frame analyses of cine films obtained with microscope and a high speed camera. Fried and Lemmer[8] studied the flow velocity field induced by *Epistylis*. They presumed that the suction flow was axially symmetric and estimated the inflow of suction produced by a single cell. This flux was approximately 10^6 μm^3/s or 1 nl/s. The other type of velocimetry image-based method is particle image velocimetry (PIV), an optical method to measure velocities by calculating the correlation between two images. Hartmann *et al.*,[9] Kowalczyk *et al.*,[10] Petermeier *et al.*,[11] and Kondratieva *et al.*[12] applied PIV to microorganisms and studied flow fields created by *Opercularia asymmetrica*. They measured 2D two-component flows in the vicinity of the microorganism. Since their measurements were limited to two dimensions, they assumed that the suction flow was axially symmetric to obtain the inflow induced by *Opercularia*. The calculated inflow was within the order of magnitude of 1nl/min, corresponding to a few hundred pl/s.

Malkiel *et al.*[13] used 3D-PTV and studied the 3D flow field generated by *Copepod* with a holography system. Although this technique is effective for a macroscopic setup, there are difficulties associated with the application of this method to a microscopic setup due to the dimensions of the equipment. Kinoshita *et al.*[14] developed a confocal micro-PIV system by combining a confocal microscope PIV system and a piezoscanner, and they measured the 3D internal flow of a moving droplet. The system reduces the thickness of the focal plane and enables them to perform 3D measurements of the flow by scanning with the thin focal plane. This technique is effective for examining microscale flows, but has not yet been applied to the study of flows generated by microorganisms.

Here we have adopted this technique to measure the flow around a microorganism. Since prolonged laser exposure is detrimental to the microorganism, we shortened the irradiation time to minimize adverse effects. We measured the 3D two components of velocities and obtained the volume flux generated by a single *Vorticella*.

II. METHODS

A. Microbiological preparation

Vorticella picta was collected from Lake Hattyou in Yoshimi, Saitama. We isolated *V. picta* and cultivated them in a culture medium containing bacteria at around 25 °C. We kept 18

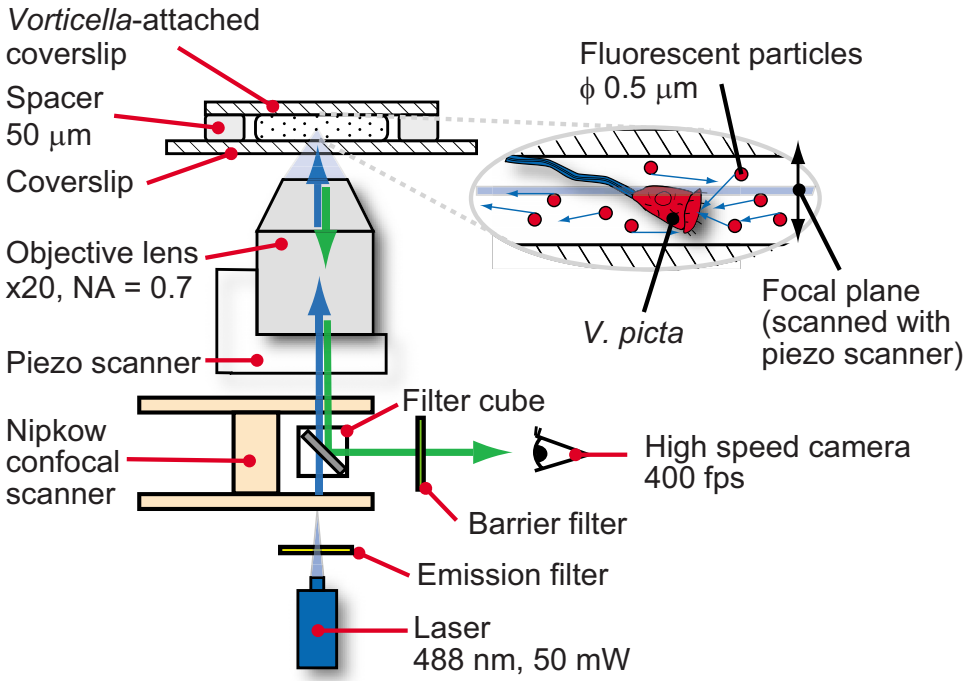

FIG. 1. A schematic of the present experimental setup to observe a flow induced by *V. picta*.

$\times 18$ mm^2 coverslips (thickness: 0.12–0.17 mm; Matsunami Glass Ind., Ltd., Osaka, Japan) floating on the culture medium for a few days until a suitable number of *V. picta* attached onto the coverslips. We made a filtered infusion of dry yeast (EBIOS, Asahi Food & Healthcare, Ltd., Tokyo, Japan) as shown below and used it for the culture medium. The medium was infused by autoclaving 2.5 g/l of EBIOS in de-ionized water passed through a Milli-Q water system (Milli-Q water, Milli-pore, Billerica, MA) at 120 °C for 20 min. Then the infused liquid was filtered through a 0.2 μm filter unit (NALGENE® Disposable Filter Unit, 566–0020; capacity: 500 ml; Nalgene, Rochester, NY) to remove solid materials. Prior to experiment, we diluted this filtered liquid tenfold with de-ionized water and used it as the culture medium.

B. Flow tracers

Since a high speed camera requires high enough fluorescence, we used fluorescent particles 0.5 μm in diameter [FluoSpheres® carboxylate-modified microspheres, F8813, suspensions (2% solids) in water plus 2 mM sodium azide, yellow-green fluorescent (excitation/emission wavelength=505/515 nm), Molecular Probes, Inc., Eugene, OR] as the flow tracers and seeding particle. The carboxylate modification of microspheres is chosen because it is effective in preventing aggregation of the microspheres. To remove the sodium azide, prior to the experiments, we washed the particles with Dryl's solution (2 mM Na_3 citrate$\cdot 2H_2O$, 0.6 mM NaH_2PO_4, 1.4 mM Na_2HPO_4, and 1.5 mM $CaCl_2\cdot 2H_2O$) by centrifuging the particles and discarding the supernatant several times. We adjusted the final concentration of the particles for PIV measurement to 0.2% solid concentration in order to obtain a high enough spatial resolution of the flow field.

C. Observation environment and flow tracers injection

We observed a flow induced by *V. picta* in a flow chamber, as shown in Fig. 1. The flow chamber was composed of three parts: (1) The *V. picta*-attached coverslip (described in Sec. II A), which was used as the upper side of the flow chamber; (2) a coverslip of larger size than the upper side (24×36 mm^2; thickness of 0.12–0.17 mm; Matsunami Glass Ind., Ltd., Osaka, Japan) was used for the bottom side of the flow chamber; and (3) a spacer, which was sandwiched between the

two coverslips to prevent crushing the *V. picta*. We coated a piece of paper, about 30 μm thick, with silicone grease (Dow Corning Toray High Vacuum Grease, Dow Corning Toray Co., Ltd., Tokyo, Japan). After coating, the thickness of the spacer was about 50 μm and the focal plane of our observation setup could span the entire height of the solution in the flow chamber. We pipetted the solution containing flow tracers from one side of the fabricated flow chamber and removed it from the other side by capillary action using Whatman No. 2 filter paper (Qualitative Filter Papers, Standard Grades, Grade 2, Whatman plc, Maidstone, Kent, UK). We removed protruding solution from both ends of the flow chamber and waited until a unidirectional flow generated by the imbalance of surface tension between both sides of the coverslip was no longer observed.

D. Measurement

We put the flow chamber on an inverted microscope (DMIRE2, Leica Microsystems GmbH, Wetzlar, Germany) equipped with an objective lens, a high speed camera, a confocal unit, a piezoscanner, and a laser (Fig. 1). Our observation setup was nearly identical to the experimental setup of Kinoshita *et al.*[14] We used a 20× objective lens (HC PL APO 20×, numerical aperture of 0.7; Dry, Leica Microsystems, Wetzlar, Germany). The images were recorded at 400 frames/s with a high speed camera (PHANTOM, Version 7.1, Vision Research, Inc., Wayne, NJ; 12 bit, monochrome, 800×600 pixel, and maximal camera speed of up to 4800 frames/s). We collected the images at 2.5 ms intervals with an exposure time of 1.5 ms. Under these conditions, the spatial resolution was 0.568 μm/pixel (352 pixel=200 μm), which corresponds to a 455×341 μm^2 observation area in one field of view. To decrease the thickness of the focal plane, we used a high speed confocal unit (CSU22, Yokogawa Electric Corp., Tokyo, Japan). We used a laser (543-BS-A03, Melles Griot Inc., Albuquerque, NM; excitation wavelength of 488 nm) for the fluorescent illumination of the flow tracers and set the output of the laser at 50 mW. The thickness of the focal plane is 4.06 ± 0.15 μm. A Nipkow disk in the confocal unit splits the laser and enables multibeam scanning for illumination of an object associated with the entire array of pixels of the camera. In accordance with 488 nm excitation laser, we used 488Ex_Ykgw and 488Ba_Ykgw_No. 1 (Yokogawa Electric Corp., Tokyo, Japan) as emission and barrier filters. The objective lens was operated stepwise by a piezoscanner (RT3D, Yokogawa Electric Corp., Tokyo, Japan; resolution: 5 nm, repeatability: ±5 nm) from the bottom to the top. The total scanning height was set to 100 μm in 41 steps with each step height of 2.50 μm at each step. 100 μm was measured to assure that the entire height of the flow field was covered. We controlled the piezoscanner and the high speed camera synchronously to obtain 15 fluorescent micrographs at each step. A total of 615 micrographs was taken in one cycle, which required about 1.5 s. During the image acquisition, we used laser illumination to reduce the exposure time.

E. PIV analysis of obtained images and definition of Cartesian coordinate system

We selected the images where fluorescent particles were visible for flow field measurements. Fifteen images were taken at each height every 2.5 ms (400 frames/s). We then processed 14 images out of 15 images. We did not use the first of the 15 images at each height for the analysis because the first image contained noise from the actuation of the piezoscanner. The 14 images were reorganized to compose ten pairs of images with 10 ms interval (100 frames/s). We chose 10 ms for the time interval of each image pair in order to appropriately detect correlation between the image pair with the PIV algorithm and time average the obtained flow field in order to remove large fluctuations between images. We converted the 12 bit images into 8 bit images for computational analysis. Then we analyzed the image pairs and calculated the flow velocities with a software package (KONCERTO, Seika Corporation, Tokyo, Japan). The images were evaluated using a cross-correlation method. Each image was interrogated at 32×32 pixel subimages with an overlap of 75% corresponding to intervals of 16 pixels. This provided 2D velocity data at 9.09×9.09 μm resolution. We averaged the ten calculated flow fields at each height. We produced a graphical representation of these analyzed flow velocities with TECPLOT (Tecplot, Inc., Bellevue, WA). Here, we define a Cartesian coordinate system to reconstruct 3D two-component flow fields:

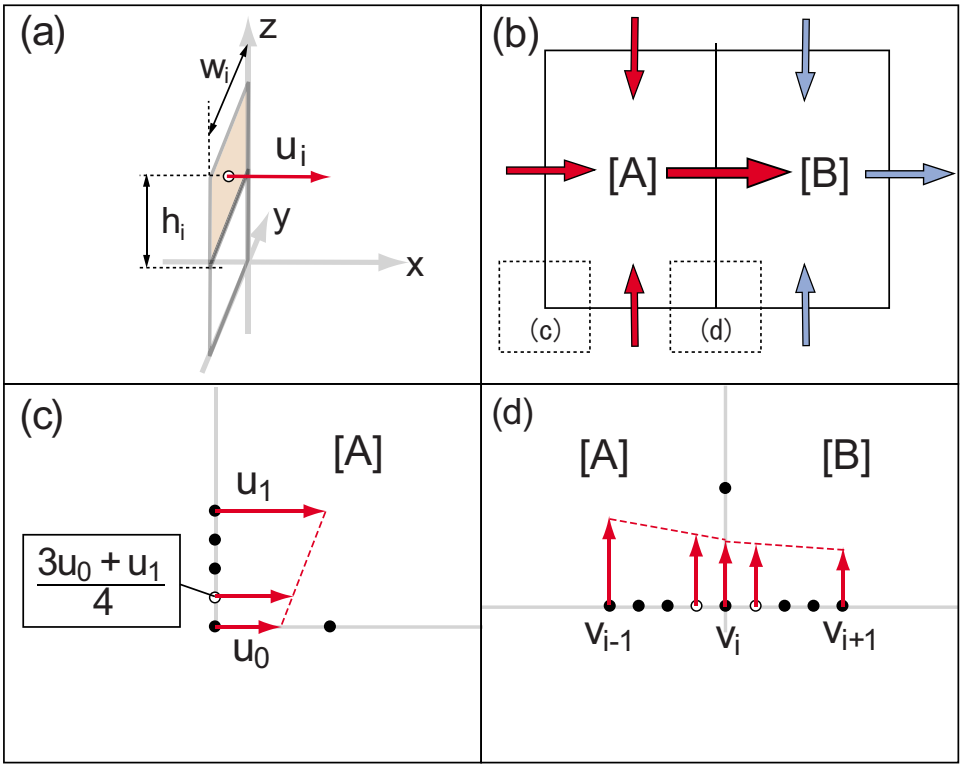

FIG. 2. A schematic illustration of calculating flow rates. (a) Flow rates were determined by the summation of the product of flow velocity normal to a surface and the area of the surface. (b) The method to calculate flow rates through a selected grid region. [(c) and (d)] The approximation method to calculate flow rates at the boundary of the grid for the edge (c) and boundary of areas *A* and *B* (d).

The *X* axis is parallel to the long side of the image, the *Y* axis is parallel to the short side of the image, and the *Z* axis is parallel to the scanning direction of the objective lens and orthogonal to the *XY* plane. The origin of this coordinate system is located at the upper left corner of the images. Moreover we set the origin of the *Z* axis at the bottom of the flow fields shown. We added height information to obtain the flow velocity field $[u_{(x,y)}, v_{(x,y)}]$ in order to reconstruct the flow field. We acquired the area, $S_{V_{\text{th}}<V_{\text{mag}}}$, where flow speeds, $V_{\text{mag}}=\sqrt{u^2+v^2}$, were greater than the threshold value of velocity V_{th} by counting each grid area (on the *XY* plane for $9.09\times9.09\ \mu\text{m}^2$ and on the *YZ* and *XZ* planes for $9.09\times2.50\ \mu\text{m}^2$). Statistical analyses such as polynomial regression were performed with MICROSOFT OFFICE EXCEL 2007.

F. Calculation of the flow rate from the obtained flow velocities

We calculated the flow rates through one plane from the obtained flow velocities. When we define a plane, the flow rate through the plane is given by

$$Q = \int_S \vec{v} \cdot \vec{n} dS, \tag{1}$$

where *S* is a defined surface, $\vec{v}$ is the velocity vector, and $\vec{n}$ is the normal vector to the surface. The flow rates are approximated by the summation of the product of the flow speed normal to the surface and the surface area, based on the obtained data (Fig. 2),

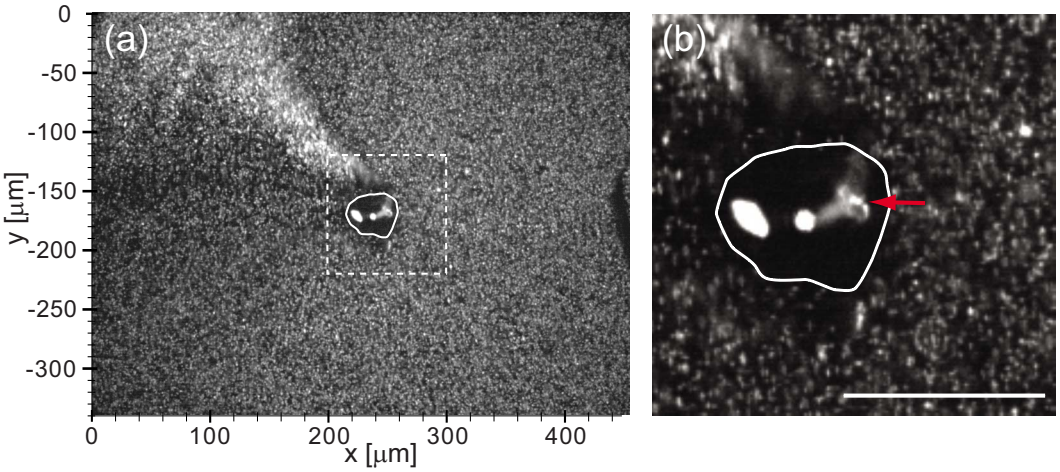

FIG. 3. A fluorescent micrograph of *V. picta* in a solution of fluorescent particles taken at $z=15$ μm. At this height, the dimensions of the *V. picta* are approximately 45 μm in width and 35 μm in height. (a) An image with our conventional coordinate system used for PIV analysis. (b) The magnified view of the region enclosed by the dashed box in (a). Red arrow indicates the infundibular organ of the *V. picta*. (Scale bar: 50 μm.)

$$Q \approx \sum_{i}^{n} u_i S_i = \sum_{i}^{n} u_i (w_i h_i), \tag{2}$$

where u_i is a flow velocity normal to a surface, S_i is the area of the surface, w_i is the width, and h_i is the height of each surface. Here w_i and h_i have the same values in our experiment. Thus, S_0 is written by

$$S_0 = w_0 h_0, \tag{3}$$

where w_0 is the interval of the data points of flow velocities, 16 pixel, i.e., 9.09 μm, and h_0 is the piezoscanning step height of 2.50 μm. Therefore S_i is always the same value, 22.7 μm^2. Since S_0 is a common term, Q is given by the following equation:

$$Q = S_0 \sum_{i}^{n} u_i. \tag{4}$$

Therefore, we can calculate flow rates by multiplication of the area and the summation of flow speeds.

We approximated flow rates at the edge of the area and at the boundary of the grids, as depicted in Figs. 2(c) and 2(d). On the edge area, we set a representative velocity at a midpoint of the area. We estimated the flow velocity on the edge area as $(3u_0+u_1)/4$, where u_0 and u_1 are the adjacent flow velocities on the edge area. We multiplied the approximated velocity by $S_0/2$ and calculated flow velocity at a representative point. The error of the approximated velocity is the discrepancy between the exact value and the approximation of the velocity. The error increases when flow speeds change drastically. On the boundary of areas A and B, we divided S_0 into two parts at the midpoint. The flow rates of both areas were approximated by multiplication of S_0 and flow speeds $(3v_{i-1}+v_i)/4$ and $(3v_i+v_{i+1})/4$, respectively, where v_{i-1}, v_i, and v_{i+1} are the adjacent flow velocities.

III. RESULTS

A. Observation of the feeding flow generated by *Vorticella*

We observed feeding flows generated by over a dozen cells of *V. picta* under laser illumination. Figure 3 shows one of fluorescent images of *V. picta* and the fluorescent particles while the

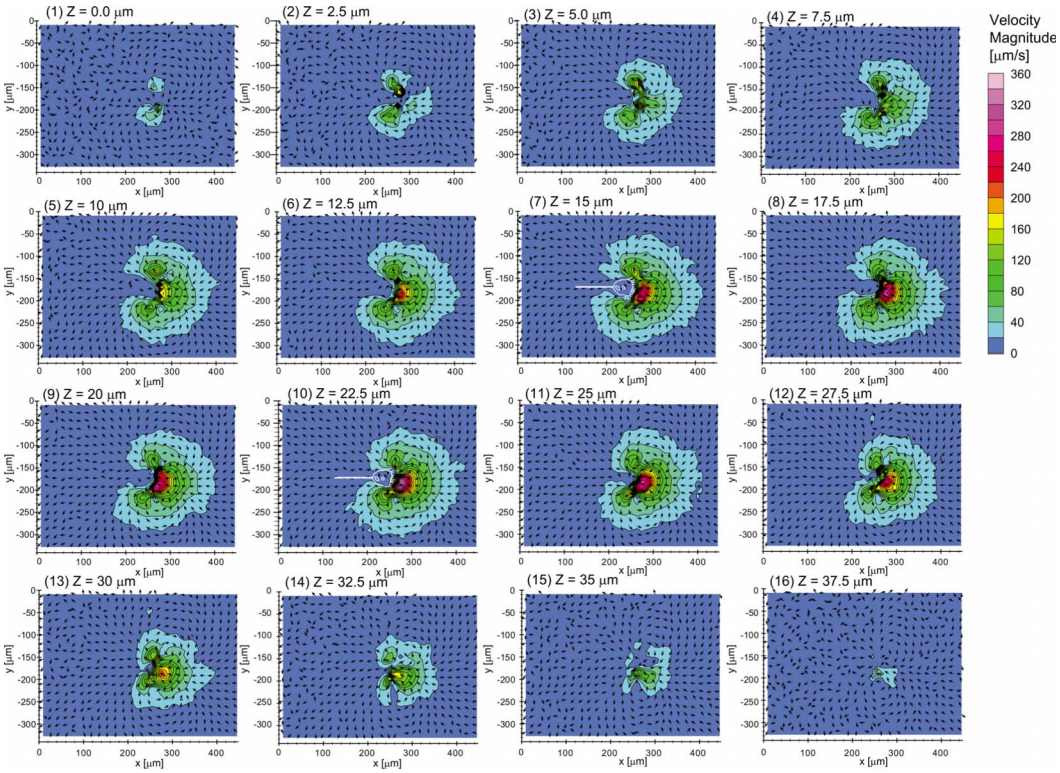

FIG. 4. [(1)–(16)] 2D two-component flow fields at each height from (1) $z=0.0$ μm to (16) $z=37.5$ μm at 2.5 μm step. Color denotes the magnitudes of the flow velocities at each point. Only half of the obtained vectors are displayed.

V. picta was feeding. The image was analyzed by the described PIV method. The cell body of the *V. picta* was at the center of the field of view. The dark area is the cytoplasmic matrix of the *V. picta* and the bright white area is its food vesicles. The dimmer white area connected to one of the food vesicles is the infundibular organ of the *V. picta*, indicated with the red arrow in the figure. Fluorescent particles were collected and distributed by the *V. picta* and the particles were ejected and accumulated in the upper left of Fig. 3. In most cases, cells of *V. picta* continued for feeding for a few seconds after the 50 mW laser illumination began. However after several seconds of laser illumination, they stopped feeding and began to contract and elongate repeatedly. When cells of *V. picta* contracted, the flow patterns changed and the particles which had been moving stopped suddenly. The only particles displaying any motion were those near the cell bodies and stalks of the cells of *V. picta*.

B. 2D two-component flow fields at different heights

We obtained 2D two-component flow velocities in the *XY* planes at different heights with the scanning PIV method described above. Here we show the 16 flow velocity fields at different heights ranging from $z=0$ μm to $z=37.5$ μm separated by a 2.50 μm interval (Fig. 4). After scanning 41 heights, fluorescent particles were visible in images taken at 18 out of the 41 heights. From these, 16 heights showed an $S_{20<V_{\mathrm{mag}}}$ greater than 1000 μm^2.

The obtained flow fields appeared symmetric with respect to a plane located between $z=17.5$ and 20 μm. At all heights, two vortices in the *XY* planes were generated in front of the oral cavity of the *V. picta*. Behind the mouth opening of the *V. picta*, the randomness of the flow direction at the top ($z=35$, 37.5 μm) and bottom regions ($z=0.0$, 2.5 μm) was higher than that in the middle region ($z=5.0$–32.5 μm). The flow field had four main characteristics in the middle part. (1) Flow toward the oral opening of the *V. picta* was generated around the cell body. (2) The

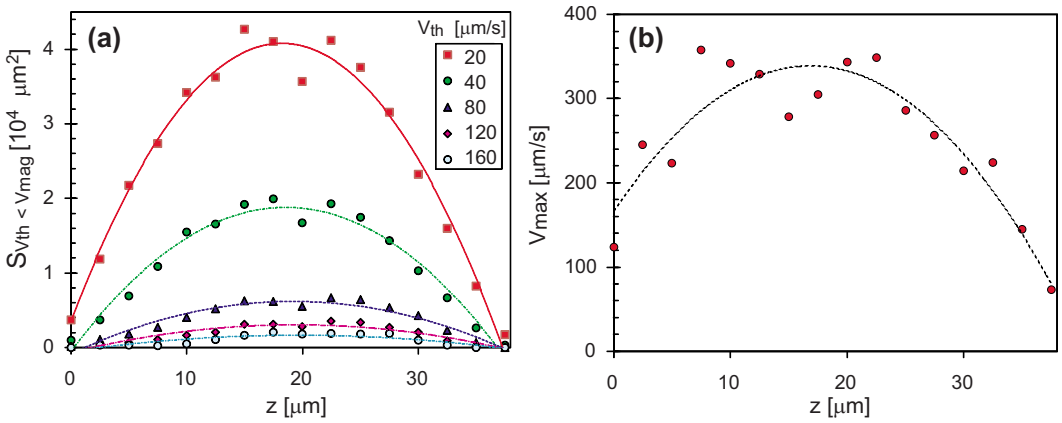

FIG. 5. Graphs of (a) feeding flow areas $S_{V_{th}<V_{mag}}$ and (b) the maximum flow speed V_{max} vs height z. The second-order polynomial fitting curves for both data sets are also indicated. All parameters of the fitting curves are shown in Table I.

strongest regions of the flow were located in front of the mouth opening and also between the two vortices on each XY planes. (3) The flow speeds increased, as the distance between the mouths of the *V. picta* decreased. (4) The flow speeds were mostly smaller than 20 μm/s in the proximity of *V. picta* cell body at distances ranging from $x=215$ to 260 μm and from $y=-155$ to -190 μm.

For convenience, we defined the feeding flow area $S_{V_{th}<V_{mag}}$, in which flow speeds were greater than a threshold flow speed V_{th}, as a parameter that indicates the size of the flow field. Another parameter is the maximum flow speed V_{max}, indicating the magnitude of the flow field. Figure 5 shows the dependence of those parameters on height z. There were three characteristics in the fitted curves of these data points. The first characteristic is that the peaks of the curves for the feeding flow area with different threshold speeds occur between $z=17.5$ and 20 μm. The second characteristic is that the curves are convex upward. The third characteristic is that the curves have the axes of symmetry going through each vortex. The relation between $S_{V_{th}<V_{mag}}$ and z can be approximated by a quadratic function curve. Coefficients of the best-fit quadratic equation, $\hat{S}_{V_{th}<V_{mag}}=a+bz+cz^2$, are shown in Table I. When the threshold flow speed is 20 μm/s, the best-fit quadratic equation is given by $3568+4085z-112.0z^2$ (coefficient of determination, $R^2=0.979$) and there is good agreement with the quadratic curve. As threshold flow speeds increased, $\hat{S}_{V_{th}<V_{mag}}$ and R^2 decreased. The maximum flow speeds are correlated with the height. The best-fit quadratic equation of the maximum flow speeds at each height is $\hat{V}_{max}=166.5+20.43z-0.6062z^2$ ($R^2=0.843$). The maximum flow speeds in the whole flow field is 357 μm/s at $z=7.5$ μm. We obtained total volumes where V_{mag} is larger than each V_{th}. When V_{th} are 20 and 40 μm/s, the total volumes are 16.6 and 7.26 pl, respectively.

TABLE I. Coefficients of the best-fit quadratic equation, $S_{V_{th}<V_{mag}}=a+bz+cz^2$, to represent the dependence of the feeding flow area $S_{V_{th}<V_{mag}}$ (μm^2) on the height z (μm). The total volumes, where V_{mag} was larger than each V_{th}, are also represented.

Threshold flow speed V_{th} (μm/s)	Intercept a	Constant b	Constant c	Coefficient of determination R^2	The total volumes where V_{mag} was larger than each V_{th} (nl)
20	3568	4085	−112.1	0.979	16.6
40	−473.7	2074	−55.90	0.969	7.26
80	−796.3	730.8	−19.05	0.937	2.35
120	−605.3	375.5	−9.682	0.872	1.12
160	−486.7	222.3	−5.670	0.766	0.598

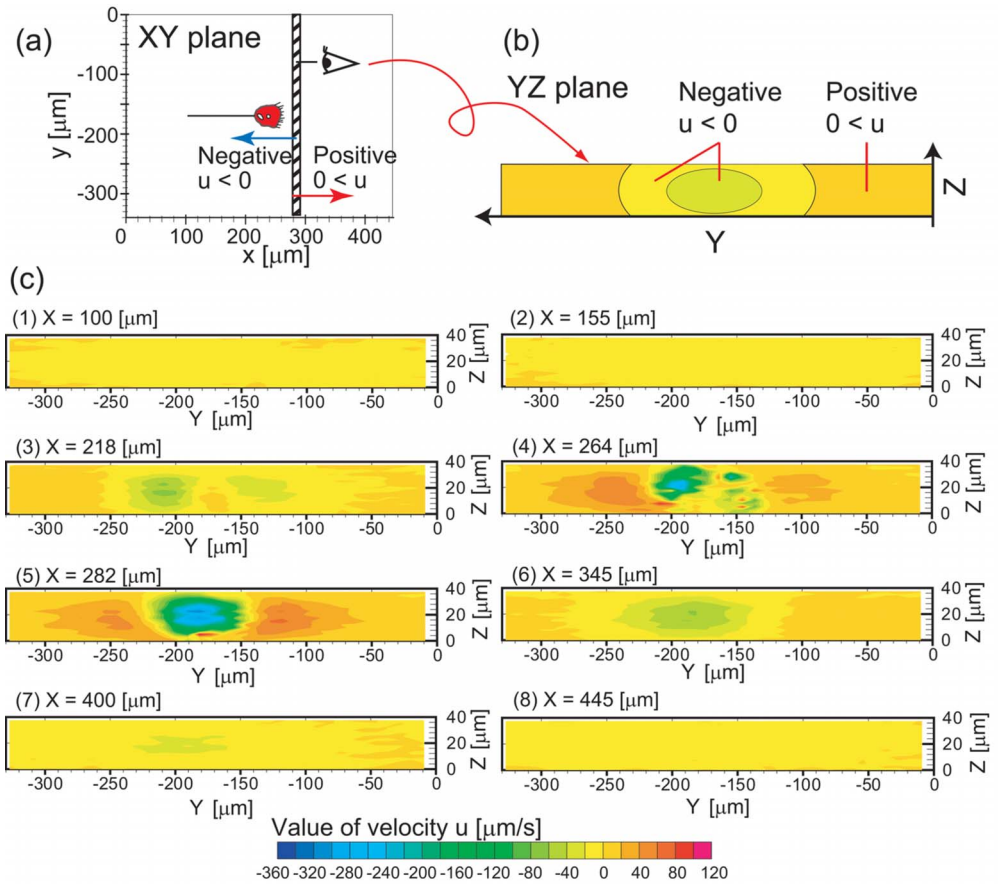

FIG. 6. Flow fields in the *YZ* planes. (a) The hatched box represents the location of the *YZ* plane. (b) Areas of the *YZ* plane are separated by color according to velocity. (c) Experimentally obtained flow fields in the *YZ* plane for eight various *X* coordinates.

C. 3D two-component flow field viewed from the *YZ* plane and flow rate through the *YZ* plane

We reconstructed flow velocity fields and visualized the flow field in the *YZ* planes for eight *X* coordinates, as shown in Fig. 6. In the vicinity of the mouth, the magnitude of flow velocities u_{mag} is greatest. Closer to the mouth, u_{mag} became larger. At $x=445$ μm, all u_{mag} are in the range of 0–20 μm/s. At $x=400$ μm, some of u_{mag} are in the range of 20–40 μm/s. Even closer to the mouth, at $x=345$ μm, some of u_{mag} were in the range of 40–60 μm/s. At $x=282$ μm, in the region adjacent to the mouth, u_{mag} was the greatest, as shown in Fig. 6. u_{mag} was greater than 200 μm/s at the center of the figure. The flow speeds near the coverslip were slower than those of the middle region between two coverslips. In the cell body of the *V. picta*, at $x=264$ μm, u was disturbed near the cell body. In the rear part, from $x=264$ μm to $x=9.09$ μm, as the distance to the mouth d_m increased, u_{mag} also decreased.

To characterize the suction flow, we focused on two values, the areas $S_{u<0}$ and the flow rate $Q_{u<0}$, which are shown in Figs. 6 and 7, respectively. In the front part of the mouth (from $x=445$ μm to $x=264$ μm), most of the values of u were negative and flow toward the mouth was generated. From $x=445$ μm to $x=264$ μm, $Q_{u<0}$ gradually increased as d_m decreased. Q_s had a peak between $x=270$ μm and $x=280$ μm in front of the mouth. The maximum magnitude of Q_s was 307 pl/s at $x=282$ μm. At $x=255$ μm, where the *YZ* plane included the cell body, Q_s had a

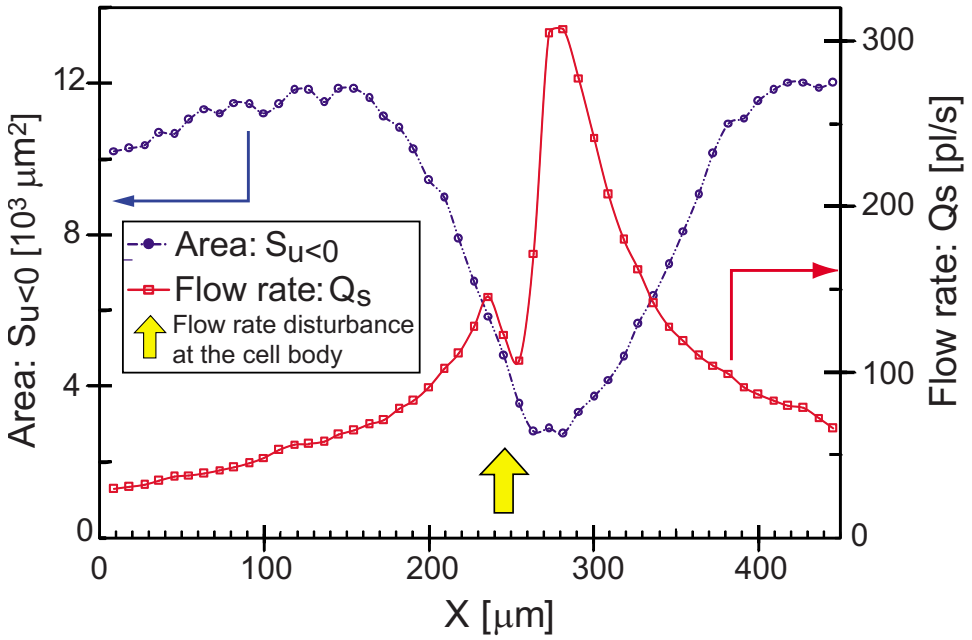

FIG. 7. A graph of the x axis distance vs the areas $S_{u<0}$ and the flow rates of suction Q_s through a YZ plane. The range $x=270-280$ μm is located in front of the mouth opening of the *V. picta*, also indicated as the yellow arrow. The entire area on a single YZ plane is 13.1×10^3 μm^2. The blue and red arrows indicate the axis of each graph.

local minimal value of 107 pl/s. In the region of $x<236$ μm and 282 $\mu m<x$, as the d_m becomes larger, the flow Q_s becomes smaller. The value of Q_s were above 20 pl/s in all observed regions from $x=9.09$ to $x=445$ μm.

From $x=445$ μm to $x=264$ μm, as d_m decreased, the size of the suction flow, $S_{u<0}$, gradually decreased and the shape of the area $S_{u<0}$ seems circular. Here, we define parenthetical percentage values as the $S_{u<0}$ percentages of the entire area of a single YZ plane, 13.1×10^3 μm. At $x=445$ μm, $S_{u<0}$ was 12.0×10^3 μm^2 (91.6%). At $x=345$ μm, $S_{u<0}$ was 7.23×10^3 μm^2 (55.2%). We also observed the boundaries between negative and positive values of u, at about $y=-280$ and -110 μm. The shapes of the areas $S_{u<-20}$ and $S_{u<-40}$ appeared circular between $x=345$ μm and $x=282$ μm. The area $S_{u<0}$ had minima around $x=260-280$ μm in the vicinity of the mouth. At the minima, the smallest value of $S_{u<0}$ was 2.75×10^3 μm^2 (21.0%). In the rear part of the mouth between $x=264$ μm and $x=9.09$ μm, as d_m increased, $S_{u<0}$ gradually increased. At $x=218$ μm, $S_{u<0}$ was 7.91×10^3 μm^2 (60.4%) and the flow determined by the body shape was observed. At $x=155$ and 100 μm, $S_{u<0}$ were 11.9×10^3 μm^2 (90.8%) and 11.2×10^3 μm^2 (85.5%), respectively. From $x=118$ μm to $x=9.09$ μm, away from the cell body, $S_{u<0}$ gradually decreased. At $x=9.09$ μm, $S_{u<0}$ was 10.2×10^3 μm^2 (77.9%).

D. Composition of flow rates of suction by *V. picta*

The amount of flow Q across a defined plane represents the components of the uptake flow of a *V. picta*. Planes are defined by points from A to F shown in Fig. 8. The plane CD is located far in front of the mouth and the plane AF far behind it. The plane BE is placed closely in front of the plane of the mouth opening. Other planes connect to the sides of those three planes. Thus, the rectangular space $ABEF$ contains the cell body, while $BCDE$ does not. The amount of influx and outflux across those planes is summarized in Table II. Across plane BE, the inflow of suction was 307 pl/s. Because some flow is recirculated from the back of the cell body, there was a flow in the reverse direction of 194 pl/s across BE. There were net influxes of 24, 63, and 26 pl/s through planes BC, CD, and DE, respectively. Outfluxes through BC, CD, and DE were below 1 pl/s. Two-thirds of inflow to $BCDE$ was supplied from the back side space $ABEF$ through the plane BE.

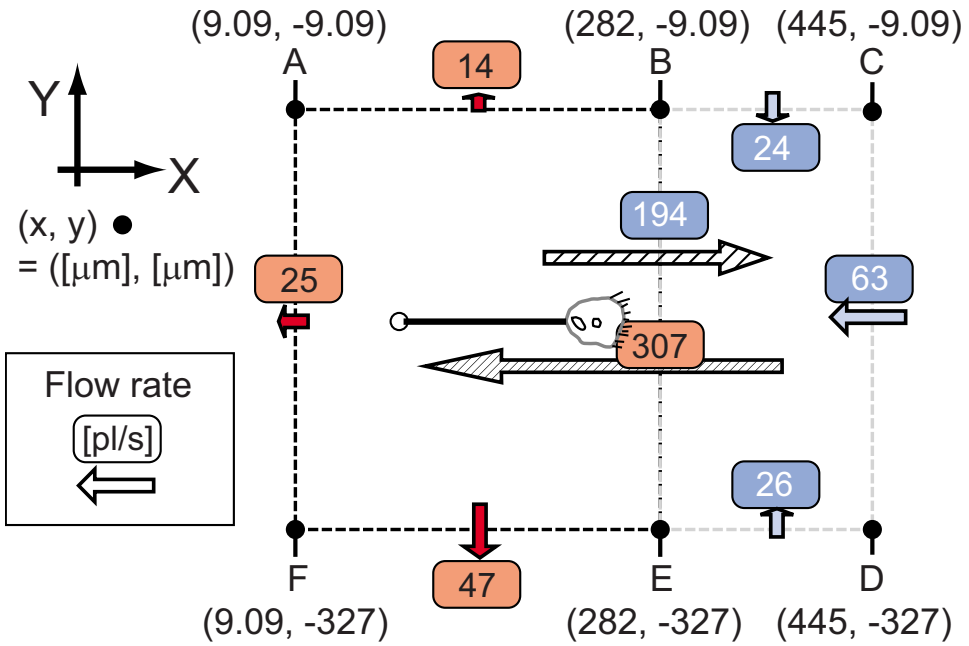

FIG. 8. The relationship of flow rates in the vicinity of a *V. picta* in two areas, *ABEF* and *BCDE*. Flow rates are given in pl/s and distances in μm. Only the total flow rates through planes are shown except the plane *BE*.

The total imbalances of flow of spaces *ABEF* and *BCDE* were 27 and 0 pl/s, respectively.

IV. DISCUSSION

The patterns of 2D two-component flow velocity fields were similar to the shape of the flow fields reported by Sleigh *et al.*[6] Their results and our results have the same characteristic shape. There exist suction flows and two vortices in front of the mouth. This flow shape is also similar to other species of stalked ciliates.[7,10–12,15] The flow fields are similar in that they both create filter-feeding currents by metachronal beating of the cilia of the paroral and oral polykinetid 1. Our measured suction inflow of 307 pl/s is close to the values generated by protozoans which are 1 nl/s (Ref. 8) and a few hundred pl/s.[9]

Laser illumination induced contractions of cells of *V. picta* and stopped their feeding. It is presumed that laser illumination provides some stimulation to *V. picta* because electrical and mechanical stimulation cause the contraction of the bodies and stalks of *V. picta*.[16] It is possible to increase the time of observation by decreasing the laser power, increasing the fluorescence of particle, and enhancing sensitivity of the camera. In Fig. 5, the area $S_{V_{th}<V_{mag}}$ and the maximum flow speed V_{max} correlates with the height z. These two values were approximated by polynomial

TABLE II. Influx and outflux through defined planes *AB*, *BC*, *CD*, *DE*, *EF*, and *FA*.

Plane	Influx (pl/s)	Outflux (pl/s)
AB	6	20
BC	25	<1
CD	64	<1
DE	27	<1
EF	1	48
FA	4	29

functions and the shape of the curve appeared parabolic and symmetric. There are four reasons for these characteristics: (1) The flow speeds become slower near boundary, (2) the normal vector to the mouth plane was almost perpendicular to the XY plane and the obtained curve appeared symmetric, (3) the *V. picta* was located at the center area of the observation, and (4) the cilia enhanced the flow field at the center and the flow field was the strongest there. Compared to $S_{V_{\mathrm{th}}<V_{\mathrm{mag}}}$, V_{max} shows some variability because these values are easily affected by a cilium, generating the flow reached at least a speed of 2500 μm/s.[6] At $x=264$ μm, the flow velocity u near the cell body was disturbed (Fig. 6). Q_s had a local minimal value of 107 pl/s at $x=255$ μm because the YZ plane there included the cell body and there was an insufficient number of fluorescent particles in the vicinity of the *V. picta* (Fig. 7). The total imbalances of flow rates through selected areas were only 27 and 0 pl/s, respectively, and show good agreement with the value of zero in Fig. 8. However the total flow rates were not balanced. We attribute this difference to the measuring error of the PIV. There are three main sources of the error: (1) Our measurement area is not fully closed, (2) on the area where flow speed changed rapidly, the flow rate has non-negligible errors because the flow rate was approximated by the sum of the product of area and average flow speed, and (3) during observation of the same height, particles moved to other planes. In addition, another factor that hinders an accurate measurement is the influence from the motion of other cells of *V. picta* outside our observed area.

Our measured flow rates are significant for understanding biological feeding strategies as we discuss below. Peritrichous ciliates feed not only on actively swimming prey organisms but also on floating organisms such as bacteria, algae, and flagellates. First, to address the feeding strategy of *V. picta* for the actively swimming organisms, we consider *Escherichia coli*, a representative actively swimming organism which swims at around 20 μm/s.[17] *V. picta* must generate sufficient area $S_{20<V_{\mathrm{mag}}}$ in its vicinity to capture the swimming organism. The area $S_{20<V_{\mathrm{mag}}}$ is around 40 000 μm^2 (Figs. 4 and 5), and the total volume is 16.6 nl. Here we suppose that the *V. picta* is hemispheroidal in shape with an equatorial radius of 18 μm and a polar radius of 40 μm. The volume is calculated to be 27 pl. Simply dividing the total volume, 16.6 nl, by the volume of a *V. picta*, 27 pl, we can determine that the *V. picta* can collect food from a fluid volume at least 615 times its volume. Next, to capture floating organisms, the flow direction rather than flow speed is important; therefore, *V. picta* is capable of capturing organisms from a volume larger than 16.6 nl. The reason why a large feeding flow is needed or produced is to allow for the capture of a sufficient number of organisms for feeding. For larger sizes of prey organisms/particles, the viscous force has a stronger effect, and the volume which *V. picta* can capture decreases. We observed the details of the suction flow to the mouth (Fig. 8).

The inflow volume to the mouth was 300 pl. 100 pl of the inflow was carried from the front of the mouth and 200 pl was brought from the rear of the mouth. Thus one-third of the volume is new liquid and two-thirds of the volume is old liquid. Two-thirds of the inflow of suction is recirculated to the front side from the rear side. The flow is circulated and the uptake of the bacteria was repeated. It is likely that the fluid circulates in this manner for the following reason: Once the flow field is generated, it is more efficient to maintain this stationary flow than to alter it because of inertia. From our data, we can obtain a clearing rate of solution per hour, which is the rate at which the organism can clear particles at low particle concentrations from a certain volume of water. We can assume that *V. picta* uptakes 100 pl/s of fresh solution from our measurements. Then, the *V. picta* clears about 360 nl/h. We divide the clearing rate per hour, 360 nl/h by the cell volume, 27 pl, and obtain clearing rate per cell volume per hour, about 1.3×10^4 1/h. This value is in agreement with the range given in Ref. 18. According to the reference, ciliates (*V. picta* is also categorized in this group) typically clear from 10^3 to 10^5 times their own volume per hour depending on the size of the feeding particle. The clearing rate of a *V. picta* is on the same order of magnitude as our measurement.

Flow generated by a microorganism is useful for the design of two types of microfluidic devices harnessing such a flow. For example, we can use *V. picta* as a microfluidic pump. If *V. picta* is encapsulated in a microchannel, the *V. picta* can work as a pump capable of generating flow of about 50 pl/s. In this case, the advantage of such a device is that the *V. picta* feeding can

be controlled with mechanical and electrical stimulation; with such stimulation, the *V. picta* can be made to stop feeding. *V. picta* also can be applied for micromixing which enhances mixing in a microfluidic channel. We are able to estimate the characteristics of such a mixer. We assume the length of one circuit of the produced vortex is 300 μm and the average flow speed is 20 μm/s. Then presuming that three cycles are sufficient to mix a 16.6 nl solution, the *V. picta* would mix at a rate of 369 pl/s.

V. CONCLUSION

We developed a method to measure the 3D two-component flow velocity field generated by a microorganism. For *V. picta*, we obtained 2D two-component flow velocity fields $[u_{(x,y)}, v_{(x,y)}]$ in the *XY* planes at different heights, by collecting such slices; we can reconstruct the 3D two-component flow velocity field $[u_{(x,y,z)}, v_{(x,y,z)}]$. We analyzed the quantitative magnitudes of the flow field, as shown in Fig. 5 and Table I. The maximum flow speeds within the entire flow field was 357 μm/s at z=7.5 μm. The total volumes in which the speeds of the flow were larger than 20 and 40 μm/s were 16.6 and 7.26 nl, respectively. From the reconstructed flow field, we visualized the suction flow in different cross sections, such as in the *YZ* planes shown in Fig. 6. We also acquired the flow rate through *YZ* and *ZX* planes and studied the composition of the suction flow produced by *V. picta* (Figs. 7 and 8 and Table II). There were two types of strong flows in front of the mouth of the *V. picta*: The inflow of suction of 307 pl/s and the reversed flow of 194 pl/s. Two-thirds of the inflow of suction was reversed to the front side from the rear, and the flow was circulated. It is efficient to maintain the stationary circulating flow. Our measurement technique provides a convenient approach for the study of other a protozoa and microorganisms. Our method opens new possibilities for the examination of biological phenomena and the characteristics of active biobased devices.

ACKNOWLEDGMENTS

We acknowledge Dr. Isamu Morishita for the identification of the *V. picta* species. We thank Dr. Albert Liau and Mr. Mauricio Cordero for useful discussions and for critical reading of the manuscript. We appreciate Mr. Yoshinori Bando at the University of Tokyo for helpful discussion of flow analysis.

[1] H. E. Buhse, Jr., J. Eukaryot Microbiol. **45**, 469 (1998).
[2] C. R. Curds, Annu. Rev. Microbiol. **36**, 27 (1982).
[3] M. J. Kim and K. S. Breuer, Anal. Chem. **79**, 955 (2007).
[4] M. J. Kim and K. S. Breuer, Small **4**, 111 (2008).
[5] K. Vopel, C. H. Reick, G. Arlt, M. Pöhn, and J. A. Ott, Aquat. Microb. Ecol. **29**, 19 (2002).
[6] M. A. Sleigh and D. Barlow, Trans. Am. Microsc. Soc. **95**, 482 (1976).
[7] M. A. Sleigh and A. Edward, Acta Protozool. **11**, 265 (1972).
[8] J. Fried and H. Lemmer, Water Sci. Technol. **47**, 189 (2003).
[9] C. Hartmann, Ö. Özmutlu, H. Petermeier, J. Fried, and A. Delgado, J. Biomech. **40**, 137 (2007).
[10] W. Kowalczyk, B. Zima, and A. Delgado, Exp. Fluids **43**, 147 (2007).
[11] H. Petermeier, W. Kowalczyk, A. Delgado, C. Denz, and F. Holtmann, Exp. Fluids **42**, 611 (2007).
[12] P. Kondratieva, J. Georgii, R. Westermann, H. Petermeier, W. Kowalczyk, and A. Delgado, Exp. Fluids **45**, 203 (2008).
[13] E. Malkiel, J. Sheng, J. Katz, and J. R. Strickler, J. Exp. Biol. **206**, 3657 (2003).
[14] H. Kinoshita, S. Kaneda, T. Fujii, and M. Oshima, Lab Chip **7**, 338 (2007).
[15] T. Fenchel, Arch. Protistenkd. **123**, 239 (1980).
[16] D. J. Patterson, Behaviour **45**, 304 (1973).
[17] N. Mittal, E. O. Budrene, M. P. Brenner, and A. van Oudenaarden, Proc. Natl. Acad. Sci. U.S.A. **100**, 13259 (2003).
[18] T. Fenchel, Microb. Ecol. **6**, 13 (1980).